Snowpack Monitoring using a Dual-Receiver Radar Architecture

Marco Pasian, *Senior Member*, *IEEE*, Massimiliano Barbolini,
Fabio Dell'Acqua, *Senior Member*, *IEEE*, Pedro Fidel Espín-López, *Student Member*, *IEEE*,
Lorenzo Silvestri, *Student Member*, *IEEE*

***Abstract* — Risk mitigation strategies to reduce the impact of avalanches on infrastructures, such as evacuation of mountain villages, and planned closure of roads, railways and ski resorts, are heavily dependent on avalanche forecasting capability. Moreover, the possibility to determine the snow water equivalent (SWE) of a snowpack is a crucial step for water management strategies used for example in agriculture and hydroelectric power plants. In both cases, for dry snow, two key physical parameters are the total snow thickness and the wave speed in the medium. Microwave radars are being used to monitor snowpacks, but they invariably invoke external aids or a-priori assumptions to calculate these physical parameters.**

This paper presents an innovative radar architecture for snowpack monitoring, of a single emitting and two receiving antennas. This novel configuration enables simultaneous identification of both total snow thickness and wave speed in the medium without any additional hypothesis or device. For dry snow, consequently, snow density and SWE can also be immediately determined. The proposed architecture is validated using first numerical simulations, then indoor and outdoor experimental results. These latter achieved accuracy levels better than 10% for total snow thickness and better than 13% for wave speed.

***Index Terms* — Downward-looking radar, FMCW radar, liquid water content (LWC), snowpack, snow avalanche, snow monitoring, snow water equivalent (SWE), upward-looking radar, wave speed.**

I. Introduction

SNOW AVALANCHES are a persistent risk for Alpine countries, threatening the safety of residents, winter tourists, and transalpine traffic [1]. Large-scale, cost-effective strategies for risk mitigation inevitably require avalanche forecasting capability to properly manage road closures, evacuations, controlled releases. In addition, because of climate change, mountain water resources are becoming increasingly critical, especially for agriculture and hydroelectric power plants [2]. Therefore, keeping track of the spatial and temporal distribution of the snow water equivalent (SWE) is vital for operational flood control, water delay planning and resource management in the snowmelt-dominated mountain basins.

In both cases, the knowledge of the local physical parameters of the snowpack is fundamental for the avalanche forecasting models and to calculate the SWE. In particular, for dry snow, two of the chief physical parameters are total snow thickness and average snow density. They are commonly measured by means of manual snowpack analysis; this latter is also normally used to return additional information, such as the internal stratigraphy and the grain types. However, manual snowpack analysis is typically feasible only at a few selected sites, and the extrapolation even to nearby sites is doubtful because of the small-scale variability of the snowpack induced by mountain topography [3]. A part of the problem is that manual analysis, albeit very precise, is extremely time-consuming. For obvious safety reasons it is rarely feasible on snow slopes exposed to the risk of avalanche release. Moreover, manual analysis is a destructive test, thus it does not easily allow for continuously monitoring the evolution of the snowpack. For these reasons, alternative solutions to complement and augment the manual analysis would be extremely beneficial, and have been investigated for a number of years.

In particular, microwave-based solutions have been proposed, including downward-looking radars [4]–[11] and upward-looking radars [12]–[18]. All these approaches offer important advantages over manual stratigraphy. Microwave measurements are not destructive, can be practically instantaneous, and can be remotely operated [19]. Moreover, upward-looking radars, buried in the ground, are considered the preferred solution for installations in the avalanche release zones, thus representing one of the few options to provide an all-weather monitoring of the most critical areas for avalanche formation. On the other hand, downward-looking radars are among the best candidates for portable systems, thus providing the possibility to rapidly acquire information over large areas, a feature useful not only for avalanche prediction, but also of great value for water management purposes, as they allow to determine the SWE of an entire mountain basin. Overall, microwave radars would perfectly complement the manual analysis. The latter would continue to provide a complete set of parameters, including the internal stratigraphy and grain types, but only at a few selected sites, normally not more than once per week. Radars would instead provide a reduced set of parameters, namely the total snow thickness, the average snow

This work was partially supported by the Italian Ministry of Education, University and Scientific Research (MIUR) under the project SIR2014 "SNOWAVE" RBSI148WE5.

M. Pasian, F. Dell'Acqua, P. F. Espín-López, and L. Silvestri are with the Dept. of Electrical, Computer and Biomedical Engineering, University of Pavia, Pavia, Italy (e-mail: marco.pasian@unipv.it; fabio.dellacqua@unipv.it; {pedrofidel.espinlopez01; lorenzo.silvestri01}@universitadipavia.it.

M. Barbolini is with the Department of Civil Engineering and Architecure, University of Pavia, Pavia, Italy and with Flow-Ing s.r.l, La Spezia, Italy (email: massimiliano.barbolini@unipv.it; m.barbolini@flow-ing.com).

density, and the SWE, but without site constraints, for any weather condition, several times per day (upward-looking) or for large areas (downward-looking).

Nevertheless, current radar prototypes show a fundamental limitation. Since the parameters of the propagation medium (snow) are generally unknown, it is not possible to calculate both the snow thickness and the wave speed from the time-of-flight of the signal obtained by a single receiver. The wave speed is related to snow dielectric permittivity, which for dry snow is a function of the average snow density. Hence, the whole problem is underdetermined. Therefore, the total snow thickness and wave speed have always been retrieved by applying information external to the radar to solve this ambiguity. In some cases, a priori assumptions on the medium dielectric properties have been used [13]–[15], [17]. In some other cases, external aids providing additional information on the snow thickness and/or physical parameters have been used, such as ultrasonic gauges, laser gauges, global positioning system (GPS) receivers, water content reflectometers, or electro-mechanical positioners to implement synthetic aperture radar (SAR) tomography, in most cases at relatively high frequencies (X and Ku band) [4]–[6], [8]–[10], [16], [20], [21]. Finally, approaches based on inverse scattering techniques and migration focusing analyses have been also proposed [7], [11], [18]. However, a priori assumptions on the average wave speed in the medium can lead to large uncertainties; additional devices considerably increase the complexity of the system while in many cases they still retain potentially large uncertainties. Moreover, additional devices are installed above ground in most cases, thus relinquishing some advantages of upward-looking radars, and considerably increasing the complexity of the system, which is a major limiting factor for the successful exploitation of these systems. Inverse scattering techniques and migration focusing analyses suffer from the non-linearity of the inversion (e.g., local minima), the need for fortuitously located diffractors (e.g., rocks), and the presence of artefacts.

This paper presents a novel approach, conceived to overcome the limitation presented above. It is based on a multi-receiver architecture, able to operate either in an upward-looking or downward looking configuration. The proposed system is built around a frequency modulated continuous wave (FMCW) radar with two independent receivers, and it calculates both the total snow thickness and wave speed in the medium without any additional assumption nor physical device. This paper is organized as follows. Section II summarizes the key dielectric properties of dry snow. Section III presents the radar architecture description. Sections IV, V, VI are related to the numerical, indoor, and outdoor validation of the system for dry snow conditions, respectively, achieving an accuracy better than 10% for the snow thickness and better than 13% for the wave speed. Finally, Section VII presents additional numerical results related to the potential use of the proposed system to investigate the structure of the internal snow layers, i.e., to calculate the snow thickness and wave speed not only for the entire snowpack, but also for the internal snow layers.

II. Dielectric Properties of Dry Snow

Several models have been developed to characterize the dielectric permittivity of the snow at microwave frequencies [22]–[27]. At the frequencies normally used for snowpack monitoring, below the Ku band, dielectric permittivity is a function of snow density and liquid water content (LWC). In particular, dry snow (LWC ~ 0 %), which can be considered a mixture of air and ice, can be described using just the real part of the dielectric permittivity. In this case, a one-to-one relationship holds between the snow density ρ and the relative dielectric constant ε', independent of frequency [24]:

$$\varepsilon' = 1 + 1.83 \cdot 10^{-3} \, \rho_{[kg/m^3]} \quad (1)$$

Typical dry snow densities for Alpine conditions range from around 90 kg/m^3 to around 450 kg/m^3. A notable exception is ice, whose density ranges between 800–900 kg/m^3. Table I summarizes the typical dry snow densities and dielectric constants. Since the imaginary part of dielectric permittivity is negligible for dry snow, it is possible to apply an approximate relation between the wave speed v and the dielectric constant ε' [28]:

$$v \sim c / \sqrt{\varepsilon'} \quad (2)$$

where c is the speed of light in vacuum. Then, combining (1) and (2), a one-to-one relationship between wave speed v and snow density ρ is obtained:

$$\rho_{[kg/m^3]} \sim 546 \, (c^2 / v^2 - 1) \quad (3)$$

Finally, the SWE is calculated according to:

$$SWE = D \, \rho / \rho_w \quad (4)$$

where D is total snow thickness and ρ_w is liquid water density (1000 kg/m^3).

III. Radar Architecture Description

The radar architecture is shown in Fig. 1 for the case of an upward-looking radar, but all considerations also hold for the case of a downward-looking radar. The building blocks are two transmitter-receiver pairs (tx–rx1 and tx–rx2) working in FMCW configuration, which is a consolidated schema for short-range applications [29].

Table I – Density, LWC, and Relative Dielectric Permittivity for Typical Dry Snow in Alpine Regions [24].

Parameter	Value
Density (kg/m^3)	90 - 450
LWC (%)	~ 0
ε'	1.16 - 1.82
ε"	~ 0

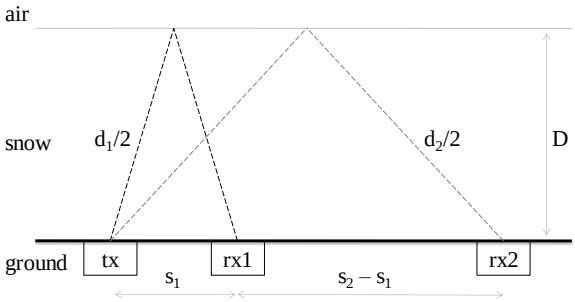

Figure 1. Radar architecture schema for the upward-looking configuration showing the transmitter (tx) and the two receivers (rx1 and rx2) installed at ground level under a snow cover with thickness D. The horizontal distance and the propagation distance are s_1 and d_1, respectively, for the first receiver, and s_2 and d_2, respectively, for the second receiver. Drawing not to scale.

For each transmitter-receiver pair the central frequency f and bandwidth B of the FMCW architecture are designed to be 2.75 GHz and 1.1 GHz (from 2.2 GHz to 3.3 GHz), respectively. These working frequencies correspond to the fundamental-mode (TE_{10}) bandwidth of standard WR340 waveguides and open-ended waveguide antennas, and achieve a penetration depth and a resolution adequate for snow heights in the order of 2 m, representing a typical condition for seasonal snow cover in the Alps [30]. To estimate the propagation loss from the transmitter to the snow/air interface and back to the receiver the radar equation and a near-field approximation for the calculation of the radar cross section of the snow/air interface are used [31], [32]. At f = 2.75 GHz the propagation loss is estimated at around 56 dB for a snow thickness of 2 m, reasonable ceiling for a typical Alpine snowpack under dry snow condition. This is calculated to be compatible with the specification of the hardware used for the experimental validation of the system, as described in Section V. For the typical snowpack conditions and system configurations, other factors, such as the reflectivity of the snow/air interface, the variations of the propagation path, and the dependence of the reflectivity itself with respect to the incidence angles, can be considered second-order effects compared to the propagation loss, thus with limited impact on the evaluation of the expected magnitude of the received signal.

With a bandwidth B = 1.1 GHz, the achievable resolution δ along the propagation path can be calculated as:

$$\delta = v/(2\mathrm{B}) \tag{5}$$

As the worst case, assuming $v = c \sim 3 \cdot 10^8$ m/s (air) and a propagation path normal to the snow/air interface (e.g., $s_1 = 0$ for tx–rx1), the resolution for snow thickness is $\delta \sim$ 13.6 cm, i.e., around 7 to 14% of the expected snow thickness for a snowpack of 1 m or 2 m, respectively. To summarize, the selected frequencies provide adequate penetration depth and adequate resolution to demonstrate the working principle of the proposed radar architecture, for dry snow under typical Alpine conditions. In addition, such frequencies are not impaired by tiny wet films, which can form close to ground, even in winter. Moreover, although this work is focused on dry snow, these frequencies can still penetrate moderately wet snowpacks, with a liquid water content (LWC) in the order of a few percent, typical of the spring season. In this case, the penetration depth is expected to be lower because of the losses due to the liquid water, but at the same time for wet snowpack a lower thickness can be usually expected, with 1 m ceiling considered to be a reasonable value for average Alpine condition. Moreover, a better equivalent resolution is expected because of the lower wave speed, resulting in similar relative resolution. It is observed that particular conditions, e.g., severe winters beyond the ordinary, leeward slopes, some Scandinavian regions, may generate snowpacks with thicknesses exceeding the limits assumed in this work, i.e. 2 m and 1 m for dry and wet snow, respectively. In this case, the central frequency f and/or the antennas can be modified to address the different conditions, if required. In addition, the bandwidth B can also be modified to achieve different resolutions. In this case, however, it should be taken into account that normally, according to (5), sharper resolutions require larger bandwidths. Larger bandwidths are however easier to achieve using antennas working at higher central frequencies, which in turn are not adequate to penetrate large thickness, especially for wet snow. Thus, a compromise is expected to be taken into account in all cases.

In any case, the real limitations of a normal FMCW radar, as anticipated, are given by the unknown wave speed in the propagation medium. According to Table I and (2), it can range from $v \sim 2.8 \cdot 10^8$ m/s ($\varepsilon' = 1.16$) to $v \sim 2.2 \cdot 10^8$ m/s ($\varepsilon' = 1.82$), thus it is centred at $2.5 \cdot 10^8$ m/s with a variability of $0.6 \cdot 10^8$ m/s (around 25%). Therefore, although the actual resolution can be as good as $\delta \sim$ 12.7 cm ($\varepsilon' = 1.16$) or $\delta \sim$ 10.1 cm ($\varepsilon' = 1.82$), the uncertainty about the wave speed is translated into an uncertainty for the snow thickness D of around 25%. As an example, for a signal time-of-flight of around 4.55 ns, the calculated snow thickness can range from around 1 m ± 5.05 cm ($\varepsilon' = 1.82$) to around 1.27 m ± 6.35 cm ($\varepsilon' = 1.16$). Moreover, according to (3), the uncertainty on wave speed is directly related to the uncertainty on snow density, which can range from around 90 kg/m^3 ($\varepsilon' = 1.16$) to around 450 kg/m^3 ($\varepsilon' = 1.82$). Consequently, the double uncertainty on the snow thickness D and density ρ corresponds, according to (4), to an uncertainty for the SWE from around 11.4 ± 0.55 cm ($\varepsilon' = 1.16$, ρ = 90 kg/m^3, D = 127 cm) to around 45 ± 2.25 cm ($\varepsilon' = 1.82$, ρ = 450 kg/m^3, D = 100 cm), showing an error in the order of 120%.

On the other hand, the use of additional aids, while often providing better results compared to the assumption of *a priori* hypotheses, exhibits its own uncertainties. For example, using techniques based on microwave devices only, an accuracy on the snow thickness up to around 20 cm has been achieved [8], [21]. As an example, with a nominal snow thickness of 1 m and snow density of 200 kg/m^3, this translates into an uncertainty of around 20% for both snow thickness and wave speed, which according to (3) and (4) increases to around 80% and 120% for the snow density and SWE, respectively.

All these problems can be in principle solved, without *a*

priori assumptions nor additional devices, working with two transmitter-receiver pairs (tx–rx1 and tx–rx2) simultaneously. In particular, the FMCW radar signal is detected by the first and second receiver after a time-of-flight T_1 and T_2, respectively:

$$T_1 = d_1 / v \quad (6)$$

$$T_2 = d_2 / v \quad (7)$$

where d_1 and d_2 are the propagation distances from the transmitter to the first and second receiver, respectively. These distances can be expressed as:

$$d_1^2 = (2D)^2 + s_1^2 \quad (8)$$

$$d_2^2 = (2D)^2 + s_2^2 \quad (9)$$

where s_1 and s_2 are the horizontal (ground-parallel) distances between the transmitter and the first and second receiver, respectively. Then, substituting (8) and (9) into (6) and (7):

$$T_1^2 = ((2D)^2 + s_1^2) / v^2 \quad (10)$$

$$T_2^2 = ((2D)^2 + s_2^2) / v^2 \quad (11)$$

The system identified by (6) and (7), which is now mathematically well-posed, can be solved for the snow thickness D and the snow wave speed *v*, with no ambiguities. Two important aspects should be mentioned. First, the analytical solution presented above can be theoretically applied to retrieve not only the snow thickness D and the wave speed *v* for the entire snowpack, but also the same information for the internal layers, thus opening the use of this type of architecture to retrieving the whole internal stratigraphy. However, this is out of the main scope for the present work. The operational bandwidth B (hence, the resolution $\delta \sim 13.6$ cm) and the separation between the receivers are intentionally designed to retrieve information related to the snowpack as a whole, and in general inadequate to discriminate internal layers. To get the approach to work for the internal layers as well, antennas with a larger bandwidth, and/or a different separation between the receivers (as discussed in Section IV) can be used, at the cost of a reduced penetration depth [33], [34]. Nevertheless, with the aim to demonstrate the potential of the proposed technique, in the following sections the internal radar traces are shown, when available, and Section VII presents numerical results related to the use of this same system, but with a different separation between the receivers.

Second, implementation in an upward-looking configuration poses some practical challenges, which can be solved using standard procedures for fixed installations in mountain areas [14], [15]. These include the deployment of the system into a trench, excavated before the winter season and sealable using waterproof boxes with a microwave-transparent windows. The power supply is often provided using automotive batteries and power-management units to control the active/sleep mode of the system to be powered, in such a way that the entire winter season can be covered. Finally, the remote control and the transmission of the measured data is usually performed using a dedicated GPRS module, which connects the installation site to a master station, conveniently located in a safe place, accessible all-year round. It is worth noting that the GPRS antenna is the only above-ground element, and for this reason it should be installed outside the expected avalanche path, e.g. on a nearby large rock, thus routing a cable from the trench to the antenna itself.

IV. Numerical Validation

The first validation of the proposed radar architecture is carried out by means of full-wave simulations. The modelled scenario is shown in Fig. 1, using open-ended WR340 waveguides as radiators, with s_1 = 30 cm and s_2 = 60 cm. These radiators, exhibiting a low gain, are suited to provide a broad illumination of the snowpack, guaranteeing that both receiving antennas collect the signal launched by the transmitting antenna, despite they are seen under different view angles, as shown in Fig. 1. From a general perspective, the separations s_1 and s_2 between the radiators are optimized according to a number of factors. Theoretically, the accuracy is improved using large mutual separations [34]. However, practical and physical compromises must be also taken into account. In particular, excessive separations are impractical because they increase the propagation distances of the signal, which in turn increases the propagation losses (thus reducing the maximum penetration depth), and because they impose logistical challenges for the outdoor tests described in Section VI, where the equipment is backpacked. For these reasons, the values of s_1 and s_2, even for the numerical tests, are limited to values compatible with the outdoor use presented in Section VI. For sake of completeness, Section VII shows the results achievable when a larger separation is viable.

With the aim of exemplifying typical operational conditions, three cases are considered. In all cases, snow thickness is D = 1 m, while density is ρ = 109 kg/m^3 (corresponding to ε' = 1.2, $v = 2.74 \cdot 10^8$ m/s, SWE = 10.9 cm), ρ = 273 kg/m^3 (corresponding to ε' = 1.5, $v = 2.45 \cdot 10^8$ m/s, SWE = 27.3 cm), and ρ = 437 kg/m^3 (corresponding to ε' = 1.8, $v = 2.24 \cdot 10^8$ m/s, SWE = 43.7 cm), respectively. Therefore, a broad spectrum of dry snow is taken into account, from low to high densities. The entire propagation medium from the transmitting antenna to the snow/air interface and back to the receiving antenna is simulated using the commercial full-wave solver Ansys HFSS, which allows taking into account non-ideal aspects, such as the antenna radiation diagram and mutual coupling. The entire signal processing chain related to the generation and de-modulation of the FMCW signal is implemented using Mathworks Matlab® routines and shown in Fig. 2. A standard saw-tooth FMCW signal $y_{in}(t)$ is synthetized, with a sweep repetition of T_s = 100 ns and a frequency span from 2.2 GHz to 3.3 GHz. Then, the signal $y_{in}(t)$ is brought to the frequency domain using a Fast Fourier Transform (FFT), thus calculating the related signal $Y_{in}(f)$.

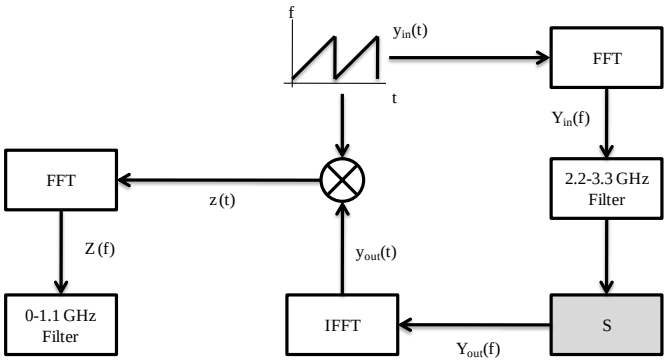

Figure 2. Block diagram of the FMCW signal processing. White blocks are related to calculations implemented in Matlab®, while the grey block provides the scattering matrix S of the propagation scenario on the basis of HFSS full-wave simulations or experimental VNA measurements for numerical and indoor/outdoor validation, respectively.

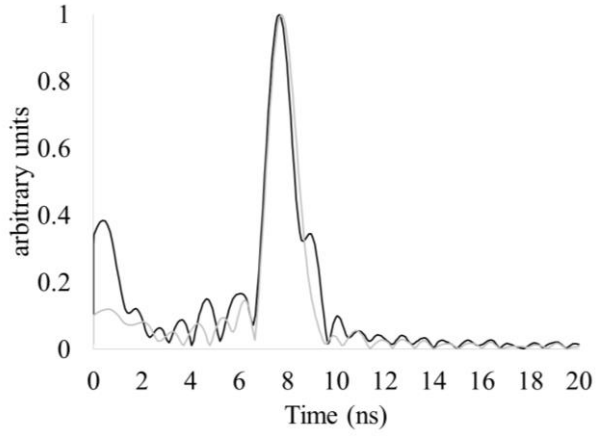

(a)

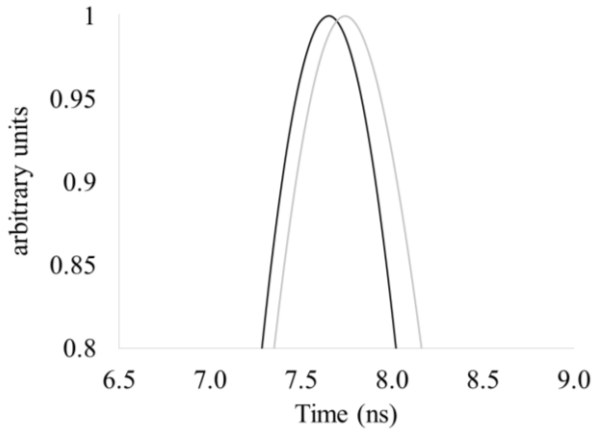

(b)

Figure 3. Numerical validation. Time-of-flight for tx–rx1 (black curve) and tx–rx2 (grey curve): (a) full scale up to 20 ns; (b) magnified view in the region of the snow/air interface.

A filter is applied to suppress all components outside the operation bandwidth (2.2-3.3 GHz) of the open-ended waveguide WR340. After this step, the signal $Y_{in}(f)$ is multiplied by the scattering matrix S calculated by the full-wave solver, which accounts for all effects related to the antennas, the snow/air interface, and to the propagation from the transmitting antenna to the receiving antenna, as anticipated at the beginning of Section IV. At the receiver side, the signal $Y_{out}(f) = Y_{in}(f) \cdot S$ is transformed back to the time domain using an Inverse Fast Fourier Transform (IFFT), obtaining $y_{out}(t)$. According to the standard FMCW processing, $y_{out}(t)$ is mixed with $y_{in}(t)$, calculating z(t). Finally, z(t) is brought to the frequency domain using a Fast Fourier Transform (FFT), calculating Z(f), and a filter as large as the bandwidth B (0 – 1.1 GHz) is applied.

As an example, the times of flight for the transmitter-receiver pairs (tx–rx1 and tx–rx2), for the case where ρ = 273 kg/m^3, are shown in Fig. 3. In particular, according to normal FMCW conversions, Z is directly shown converting the natural horizontal frequency coordinates into time-of-flight coordinates ($t = f \cdot T_s \cdot B^{-1} / 2$). For both receivers the reflection given by the snow/air interface is detected. The times of flight to the two receivers are T_1 = 7.66 ns and T_2 = 7.74 ns, respectively. According to (10) and (11), this returns D = 1.04 m and $v = 2.43 \cdot 10^8$ m/s.

The results for the three numerical cases are summarized in Table II. Errors with respect to the nominal values are less than 7% and 10% for the snow thickness and the wave speed, respectively. These parameters, referred to as the "master" parameters in Table II, i.e., the parameters obtained solving (10) and (11), exhibit errors in line with the expected resolution for the snow thickness ($\delta \sim$ 13.6 cm, around 14% for a total thickness D = 100 cm). Then, once the variable D and v are determined solving (10) and (11), the other parameters, the snow density ρ, the dielectric constant ε', and the SWE (referred to as the "derived" parameters in Table II), are directly calculated without further processing according to (3), (2), and (4), respectively. Therefore, the errors for these derived parameters are simply the errors for D and v, propagated through the non-linear relationships (3), (2), and (4).

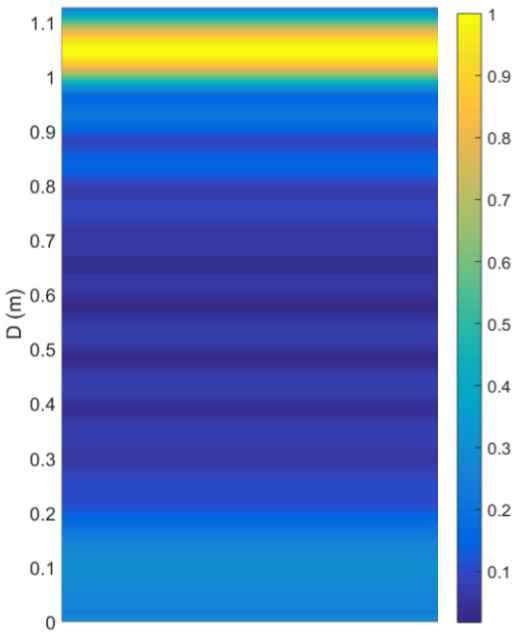

Figure 4. Radar trace (normalized magnitude of the reflected signal) for the second receiver in numerical validation, Section IV, with snow density ρ = 273 kg/m^3 and snow thickness D = 1 m.

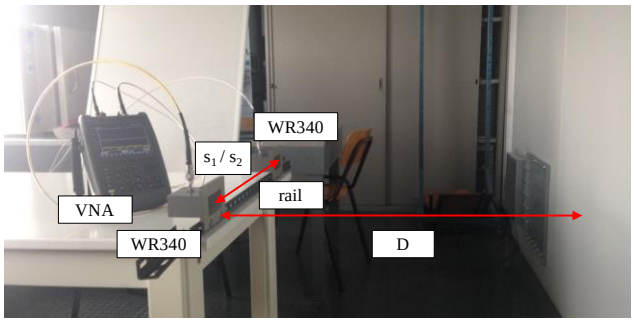

Figure 5. Experimental setup for indoor validation. Two open-ended WR340 waveguides, separated by a distance s1 or s2, are driven by a VNA. The target is a flat metal wall at a distance D with normal air (ε' ~ 1) in between. One of the two open-ended WR340 waveguides is moved to different position to mimic the presence of two receivers.

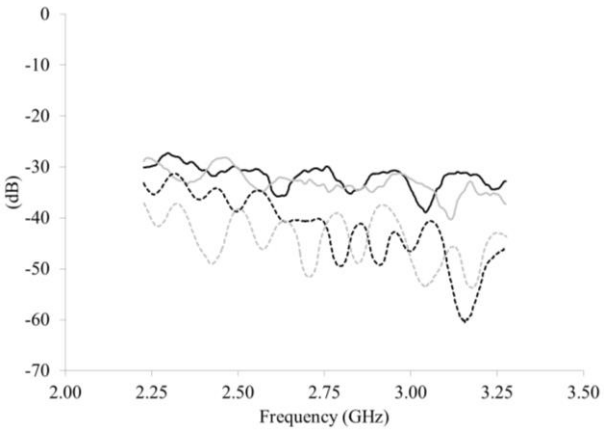

Figure 6. Magnitude of the transmission coefficient for tx-rx1 (black curves) and tx-rx2 (grey curves). Indoor validation (solid curves) and outdoor validation (dashed curves).

For completeness, Fig. 4 shows, as an example, also the radar trace for the case where ρ = 273 kg/m^3, for the second receiver at s_2 = 60 cm. It can be appreciated that the snow-air interface is identified, clearly emerging from the background.

V. Indoor Validation

The second validation of the proposed radar architecture is carried out in a controlled laboratory environment. This is mainly intended to test the radar architecture, implementation, and routines, as well as to provide a first experimental verification on the level of the received signal, having in mind that for this purpose standard air (ε' ~ 1, ε" ~ 0) can be seen as an approximation of very dry snow (ε' ~ 1.16, ε" ~ 0, Table I). The experimental setup is shown in Fig. 5. It comprises a vector network analyzer (VNA) from Keysight (FieldFox N9916A) used to generate the transmit signal, two open-ended WR340 waveguide antennas to emit the signal and receive the backscattered echo from the target, and two coaxial cables to connect the antennas with the VNA, 2 m long each. According to its datasheet, the VNA generates a maximum transmitted power of around -1 dBm and exhibits a noise floor of around -81 dBm at the frequencies of interest, using an intermediate frequency for the VNA of 10 kHz. Taking into account the maximum propagation loss calculated in Section III, around 56 dB, this ideally returns a minimum margin of around 25 dB for the signal-to-noise ratio. In addition, the intermediate frequency of 10 kHz allows for a measurement time of around 0.8 s (with 1001 discrete points from 2.2 GHz to 3.3 GHz). The target is a solid metal wall at 1-meter distance from the antenna plane, accurately measured using a high-precision laser range meter (Hilti PD28) with a datasheet accuracy of ±2.1 mm.

The antennas are mounted on a metal rail. Taking advantage of the static nature of the target, this allows implementing the two-receiver architecture using just a single receiving antenna, which is manually translated along the rail in two different positions. Using this solution, it is possible to mimic two receiving antennas at distances s_1 = 30 cm and s_2 = 60 cm from the transmitter, avoiding a more expensive implementation based on two independent receiving antennas placed at two fixed distances from the transmitter. This experimental test can be seen as an extreme case of dry snow, the propagation medium being standard air with negligible losses (ε' ~ 1, ε" ~ 0).

The times of flight T_1 and T_2 are calculated using the FMCW routines developed in Matlab, as explained in Section IV and shown in Fig. 2. In this case, the scattering matrix is experimentally acquired by the VNA. The magnitude of the transmission coefficients for both the transmitter-receiver pairs (tx–rx1 and tx–rx2) are shown in Fig. 6.

The observed signal strength is within the range of the analytical predictions discussed in Section III, with a minimum value around -35 dB at 2.75 GHz. The variability of the transmission coefficients as a function of frequency (Fig. 6), which is typical of propagation within complex media, does not impair radar operation because the method is based on the time of flight between the antennas and the interfaces, not directly on the magnitude of the backscattered signal.

After applying the FMCW signal processing shown in Fig. 2 and discussed in detail in Section IV, the time of flight related to the metal wall reflection is calculated, and (10) and (11) are used to obtain D = 0.98 m and v = 2.96·10^8 m/s. Consequently, the calculated dielectric constant is ε' = 1.03. Accordingly, the medium density and SWE are close to zero (ρ = 15 kg/m^3 and SWE = 1.5 cm, respectively), as expected. Both for the target distance and the wave speed, the error relative to the nominal values is less than 2%, as reported in Table II.

VI. Outdoor Validation

The third and latest validation of the proposed radar architecture is carried out in real field tests, on slopes in the Italian Alps (Valle d'Aosta). Two experimental sites are close to Pila, at 45°40'36" N 7°19'40" E and 45°40'30" N 7°19'35" E, around 2500 m above sea level, with an inclination θ_1=25 deg and θ_2=27 deg, respectively. The third experimental site is close to Cervinia, at 45°55'14" N 7°41'34" E, around 3000 m above sea level, with an inclination θ_3=10 deg. Our experiments were conducted in February and March 2017, and then in April 2018, and the setup is shown in Fig. 7. This latter is based on the same devices described in Section V, with a different rail, more suited to the outdoor scenario.

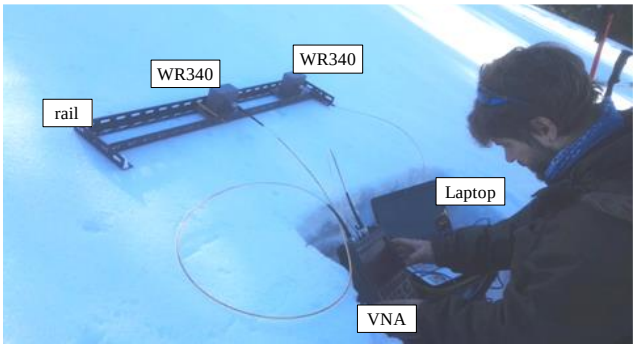

Figure 7. Experimental setup for the outdoor validation, similar to the setup shown in Fig. 5, in a downward looking configuration. A different rail, suited for the outdoor validation, is adopted. The target is represented by the snow cover (ε' = 1.39) directly below the rail, shown after the manual analysis in Fig. 8.

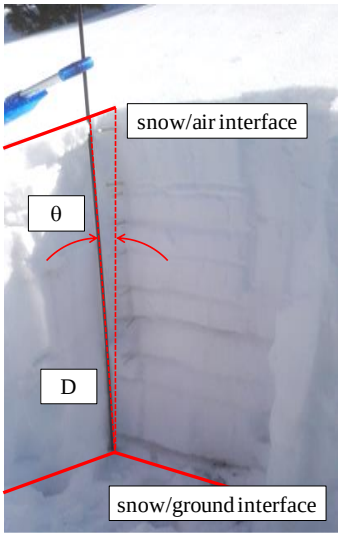

Figure 8. Experimental site for the outdoor validation. The snow cover directly below the rail shown in Fig. 7 was excavated to the ground, and manual analysis performed. Because of the inclination of the slope (θ = 27 deg), it can be appreciated the difference between the snow cover height (1.25 m) and thickness (D = 1.11 m).

Moreover, this experimental validation was based on a downward-looking configuration to ease the logistic aspects.

As for the indoor validation, the times of flight T_1 and T_2 are calculated using the FMCW routines developed in Matlab, as explained in Section IV and shown in Fig. 2, and the scattering matrix is experimentally acquired by the VNA. With a minimum value of around -50 dB at 2.75 GHz, the magnitudes of the transmission coefficients for both transmitter--receiver pairs (tx–rx1 and tx–rx2, Fig. 6) lie within the analytical predictions discussed in Section III.

After the radar measurements, a manual snowpack analysis took place, care of professional chartered AINEVA experts, as shown for example in Fig. 8 for the March 2017 test. In particular, the site of the radar measurements was excavated down to the solid ground, and the snowpack was analysed identifying each and all layers, and measuring for each of them the thickness, density, and LWC. This latter was found to be negligible for the entire snowpack, which was consequently considered in dry snow condition. The results of the manual snowpack analysis returned snow heights (measured parallel to the gravity vector) of 1.27 m, 1.25 m, and 1.67 m for February 2017, March 2017, and April 2018, respectively. The corresponding snow thicknesses (measured normal to the ground), calculated taking into account the inclination of the slope, as shown in Fig. 8, are D = 1.15 m (1.27 $\cos\theta_1$), D = 1.11 m (1.25 $\cos\theta_2$), and D = 1.64 m (1.67 $\cos\theta_3$) for February 2017, March 2017, and April 2018, respectively. The other parameters are ρ = 257 kg/m^3 and SWE = 29.6 cm (corresponding to ε' = 1.47, $v = 2.47\cdot10^8$ m/s) for February 2017, ρ = 253 kg/m^3 and SWE = 28.1 cm (corresponding to ε' = 1.46, $v = 2.48\cdot10^8$ m/s) for March 2017, and ρ = 339 kg/m^3 and SWE = 55.6 cm (corresponding to ε' = 1.62, $v = 2.36\cdot10^8$ m/s) for April 2018. After applying the FMCW signal processing shown in Fig. 2 and discussed in details in Section IV, the time-of-flight for the first and second receiver related to the reflection at the snow/ground interface was calculated, and (10) and (11) were used to obtain D and v for the outdoor test cases. The results are summarized in Table II. The error of the master parameters, with respect to the nominal values, is less than 10% and 13% for the snow thickness and the wave speed, respectively. Again, these errors are in line with the expected resolution for snow thickness (δ ~ 13.6 cm, around 12% for a total thickness D = 115 cm), while the errors for the derived parameters, snow density ρ, dielectric constant ε', and SWE, are simply the errors achieved for D and v, propagated through the non-linear relationships (3), (2), and (4).

In addition, Fig. 9, as an example, shows the radar trace for the outdoor validations taken in 2017 for the second receiver. Not only the reflection at the snow-ground interface is identified, but also the internal interfaces, given by the stratigraphy of the snowpack, are detected. Note that these radar traces are shown for illustrative purposes only. The current experimental setup is not designed to measure the physical and dielectric parameters of the internal layers. Section VII discusses how the same system, with a larger separation between the receivers, can be used to obtain corresponding information for the internal snow layers.

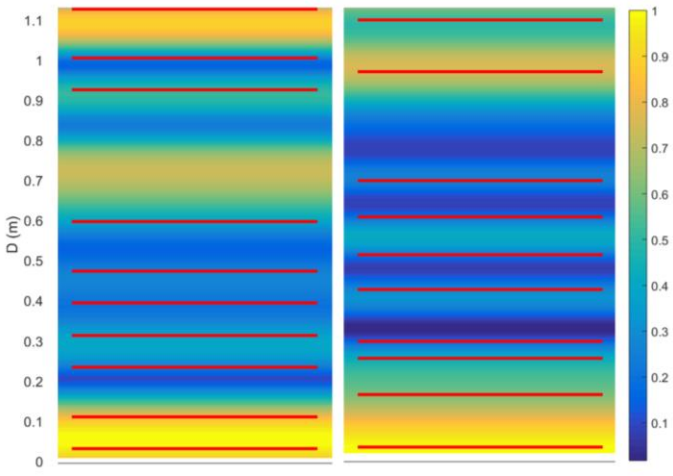

(a) (b)

Figure 9. Radar traces (normalized magnitude of the reflected signal) for the second receiver in outdoor validation, Section VI: (a) February 2017; (b) March 2017. Red lines represent the location of interfaces as determined by the manual snow cover analysis.

TABLE II – VALIDATION RESULTS.

	Numerical			Indoor	Outdoor		
	1	2	3		1	2	3
	nominal						
Thickness D [cm]	100	100	100	100	115	111	164
Wave speed v [m/s]	$2.74 \cdot 10^8$	$2.45 \cdot 10^8$	$2.24 \cdot 10^8$	$3 \cdot 10^8$	$2.47 \cdot 10^8$	$2.48 \cdot 10^8$	$2.36 \cdot 10^8$
Density ρ [kg/m^3]	109	273	437	0	259	253	339
Dielectric constant ε'	1.2	1.5	1.8	1	1.47	1.46	1.62
SWE [cm]	10.9	27.3	43.7	0	29.8	28.1	55.6
	calculated						
Thickness D [cm]	101	104	93	98	124	100	158
Wave speed v [m/s]	$2.63 \cdot 10^8$	$2.43 \cdot 10^8$	$2.02 \cdot 10^8$	$2.96 \cdot 10^8$	$2.79 \cdot 10^8$	$2.54 \cdot 10^8$	$2.27 \cdot 10^8$
Density ρ [kg/m^3]	164	286	658	15	85	216	407
Dielectric constant ε'	1.30	1.52	2.2	1.03	1.16	1.39	1.74
SWE [cm]	16.6	29.7	61.2	1.5	10.5	21.6	64.3
	accuracy for master parameters [%]						
Thickness D	1	4	7	2	8	10	4
Wave speed v	4	1	10	2	13	3	4
	accuracy for derived parameters						
Density ρ [kg/m^3]	55	13	221	15	-174	-37	68
Dielectric constant ε'	0.1	0.02	0.4	0.03	-0.31	-0.07	0.12
SWE [cm]	5.7	2.4	17.5	1.5	-19.3	-6.5	8.7

TABLE III – VALIDATION RESULTS FOR INTERNAL SNOW LAYERS

	Layer 1	Layer 2	Layer 3	Layer 4	Layer 5	Total
	nominal					
Thickness D [cm]	20	20	25	15	56	136
Wave speed v [m/s]	$2.74 \cdot 10^8$	$2.63 \cdot 10^8$	$2.45 \cdot 10^8$	$2.24 \cdot 10^8$	$2.34 \cdot 10^8$	$2.43 \cdot 10^8$
Density ρ [kg/m^3]	109	164	273	437	355	285
Dielectric constant ε'	1.2	1.3	1.5	1.8	1.65	1.52
SWE [cm]	2.2	3.3	6.8	6.6	19.9	38.7
	calculated					
Thickness D [cm]	21	17	25	n.a.	61	124
Wave speed v [m/s]	$2.79 \cdot 10^8$	$2.38 \cdot 10^8$	$2.27 \cdot 10^8$	n.a.	$2.50 \cdot 10^8$	$2.59 \cdot 10^8$
Density ρ [kg/m^3]	87	322	404	n.a.	240	188
Dielectric constant ε'	1.16	1.59	1.74	n.a.	1.44	1.34
SWE [cm]	1.8	5.5	10.1	n.a.	14.7	23.3
	accuracy for master parameters [%]					
Thickness D	5	15	0	n.a.	9	9
Wave speed v	2	10	7	n.a.	7	6
	accuracy for derived parameters					
Density ρ [kg/m^3]	-22	158	131	n.a.	-115	-97
Dielectric constant ε'	-0.04	0.29	0.24	n.a.	-0.21	-0.18
SWE [cm]	-0.4	2.2	3.3	n.a.	5.2	-15.5

VII. Potential of the Approach for the Internal Snow Layers

The proposed system can also in principle be used to calculate snow thickness and wave speed for the internal snow layers. One has to solve (10) and (11) for each internal interface determining the snow thickness and wave speed for the first layer, then using this information in a nested solution to determine snow thickness and wave speed for the second layer, and so on. In order to improve the accuracy, the operational bandwidth B (hence, the resolution δ) and/or the separation between the receivers should be enlarged, [33], [34]. To demonstrate the potential of the proposed technique for investigating the internal structure of the snowpack, in this section a fictitious snowpack is analysed numerically, using a larger separation between the receivers (s_1=30 cm and s_2=100 cm).

The results are summarized in Table III, while radar traces for the two receivers are shown in Fig. 10. In particular, several internal reflections are detected, and the selection of the different pairs (for example, the pair 10.7/11.5 ns for the snow-ground reflection) is done manually. Even if automatic detection algorithms could be implemented in order to simplify and speed up the process, taking into account that the automatic identification of the internal interfaces is expected to be more complicated compared to the identification of the snowpack interfaces (snow-ground or snow-air), we chose to stay on the safe side and rely on manual selection.

This numerical test is carried out on a snowpack composed of five different layers, with thickness ranging from 15 cm to 56 cm (total thickness 136 cm). Four different snow layers are identified. Only the thinnest layer (Layer 4), whose thickness approaches the limit imposed by the operational bandwidth, is not identified. For all the other layers, the accuracy of the master parameters is better than 15% and 10% for the snow thickness and wave speed, respectively.

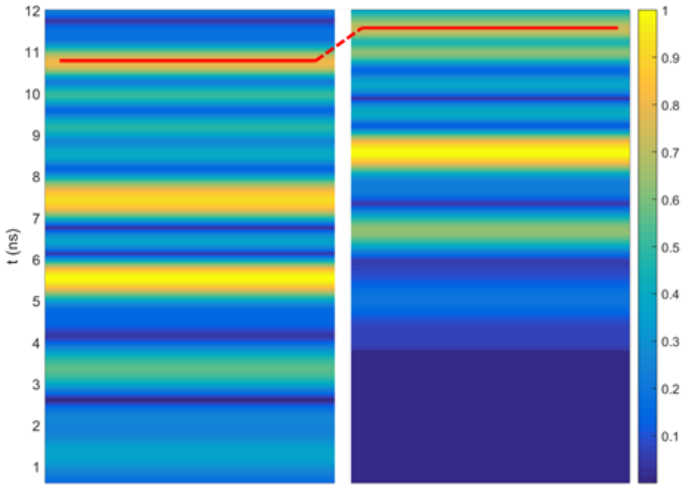

(a) (b)

Figure 10. Radar traces (normalized magnitude of the reflected signal) for the (a) first and (b) second receiver for the numerical validation for the internal snow layers, Section VII. As an example, the red lines identify the pair related to the ground-snow reflection, which occurs at 10.7 ns and 11.5 ns for the first and second receiver, respectively.

Again, the errors for the derived parameters, snow density ρ, dielectric constant ε', and SWE, are simply the errors achieved for D and v, propagated through the non-linear relations (3), (2), and (4).

Finally, when the internal stratification is accounted for, the propagation path between the transmitter and the receivers can be modelled more precisely taking into account the different diffraction angles due to Snell's Law. Although in most practical cases the angle difference is rather limited [5] [6], a second-order correction may be implemented to take into account this effect and refine the results.

VIII. Conclusions

This paper presented a novel radar architecture for snowpack monitoring, based on the simultaneous use of two receivers. This approach is capable of overcoming the basic limitations of single-receiver designs at microwave frequencies, calculating both total snow thickness and wave speed in the medium (used in turn to calculate the snow density and SWE for dry snow), without any *a priori* hypothesis or external device. The proposed architecture was validated using numerical simulations, a controlled laboratory setup, and real field test experimental site, demonstrating an overall accuracy better than 10% for total snow thickness and better than 13% for wave speed, in agreement with theoretical expectations.

The working principle was demonstrated, and the possibility of installation either upward-looking or downward-looking was discussed. However, the subsequent calculation of derived parameters, such as snow density, dielectric constant, and SWE, on the grounds of the accuracy achieved for the snow thickness and wave speed, demonstrated margins of improvement to meet operational requirements.

Acknowledgements

The authors would like to thank *Fondazione Montagna Sicura – Montagne Sûre* and *Regione Autonoma Valle d'Aosta – Région Autonome Vallée d'Aoste* for their valuable support to the field activities.

References

[1] K. Lied, SATSIE Avalanche Studies and Model Validation in Europe – Final Report, European Commission 5th Framework Programme, May 31, 2006.

[2] D. Viviroli, D. R. Archer, W. Buytaert, H. J. Fowler, G. B. Greenwood, A. F. Hamlet, Y. Huang, G. Koboltschnig, M. I. Litaor, J. I. Lopez-Moreno, S. Lorentz, B. Schadler, H. Schreier, K. Schwaiger, M. Vuille, and R. Woods, "Climate change and mountain water resources: overview and recommendations for research, management and policy," *Hydrology and Earth System Sciences*, Vol. 15, pp. 471–504, 2011

[3] H.-P. Marshall and G. Koh, "FMCW Radars for snow research," *Cold Regions Science and Technology*, Vol. 52, pp. 118–131, 2008.

[4] O. Frey, C. L. Werner, and A. Wiesmann, "Tomographic profiling of the structure of a snow pack at X-/Ku-Band using SnowScat in SAR mode," *2015 European Microwave Conference*, Paris, France, September 6–11, 2015.

[5] B. Rekioua, M. Davy, and L. Ferro-Famil, "Snowpack characterization using SAR tomography - experimental results of the AlpSAR campaign," *2015 European Radar Conference*, Paris, France, September 6–11, 2015.

[6] B. Rekioua, M. Davy, L. Ferro-Famil, and S. Tebaldini, "Snowpack permittivity profile retrieval from tomographic SAR data," *Comptes Rendus Physique*, Vol. 18, pp. 57–65, 2017.

[7] J. H. Bradford, J. T. Harper, and J. Brown, "Complex dielectric permittivity measurements from ground-penetrating radar data to estimate snow liquid water content in the pendular regime," *Water Resources Research*, Vol. 45, pp. 1–12, 2009.

[8] K. Morrison and J. Bennett, "Tomographic Profiling—A Technique for Multi-Incidence-Angle Retrieval of the Vertical SAR Backscattering Profiles of Biogeophysical Targets," *IEEE Transactions on Geoscience and Remote Sensing*, Vol. 52, No. 2, pp. 1350–1355, February 2014.

[9] Y. Yamaguchi, M. Mitsumoto, M. Sengoku, and T. Abe, "Synthetic aperture FM-CW radar applied to the detection of objects buried in snowpack," *IEEE transactions on geoscience and remote sensing*, Vol. 32, No. 1, pp. 11–18, 1994.

[10] J. Holmgren, M. Sturm, N. E. Yankielun, and G. Koh, "Extensive measurements of snow depth using FM-CW radar," *Cold Regions Science and Technology*, Vol. 27, No. 1, pp. 17–30, 1998.

[11] W. S. Holbrook *et. al*., "Estimating snow water equivalent over long mountain transects using snowmobile-mounted ground-penetrating radar," *Geophysics*, Vol. 81, No. 1, pp. WA213–WA223, January-February 2016.

[12] H. Gubler and M. Hiller, "The use of microwave FMCW radar in snow and avalanche research," *Cold Regions Science and Technology*, Vol 9, pp. 109–119, 1984.

[13] C. Mitterer, A. Heilig, J. Schweizer, and O. Eisen, "Upward-looking ground-penetrating radar for measuring wet-snow properties," *Cold Regions Science and Technology*, Vol. 69, pp. 129–138, 2011.

[14] R. Okorn, G. Brunnhofer, T. Platzer, A. Heilig, L.Schmid, C. Mitterer, J. Schweizer, and Olaf Eisen, "Upward-looking L-band FMCW radar for snow cover monitoring," *Cold Regions Science and Technology*, Vol. 103, pp. 31–40, 2014.

[15] L.Schmid, A. Heilig, C. Mitterer, J. Schweizer, H. Maurer, R. Okorn, and O. Eisen, "Continuous snowpack monitoring using upward-looking ground-penetrating radar technology," *Journal of Glaciology*, Vol. 60, No. 221, pp. 509–525, 2014.

[16] A. Heilig, M. Schneebeli, and O. Eisen, "Upward-looking ground-penetrating radar for monitoring snowpack stratigraphy," *Cold Regions Science and Technology*, Vol. 59, pp. 152–162, 2009.

[17] A. Heilig, O. Eisen, and M. Schneebeli, "Temporal observations of a seasonal snowpack using upward-looking GPR," *Hydrological Processes*, Vol. 24, pp. 3133–3145, 2010.

[18] L. Schmid *et. al*., "A synthetic study to assess the applicability of full-waveform inversion to infer snow stratigraphy from upward-looking ground-penetrating radar data," *Geophysics*, Vol. 81, No. 1, pp. 1–11, January-February 2016.

[19] R. Persico, *Introduction to Ground Penetreting Radar*, IEEE Press – Wiley, Hoboken, New Jersey, U.S.A., 2014.

[20] A. Godio, D. Franco, B. Chiaia, B. Frigo, L. Dublanc, M. Freppaz, M. Maggioni, E. Ceaglio, and P. Dellavedova, "Seasonal monitoring of snow properties by WCR and up-GPR," *21st European Meeting of Environmental and Engineering Geophysics – Near Surface Geoscience 2015*, Turin, Italy, September 6–10, 2015.

[21] L.Schmid, F. Kock, A. Heilig, M. Prasch, O. Eisen, W. Mauser, and J. Schweizer, "A novel sensor combination (upGPR-GPS) to continuously and nondestructively derive snow cover properties," *Geophysical Research Letters*, Vol. 42, 2015.

[22] M. E. Tiuri, A. H. Sihvola, E. G. Nyfors, and M. T. Hallikainen, "The complex dielectric constant of snow at microwave frequencies," *IEEE Journal of Oceanic Engineering*, Vol. OE-9, No. 5, pp. 377–382, December 1984.

[23] A. Sihvola, E. Nyfors, and M. Tiuri, "Mixing formulae and experimental results for the dielectric constant of snow," *Journal of Glaciology*, Vol. 31, No. 108, pp. 163–170, 1985.

[24] M. T. Hallikainen, F. T. Ulaby, and M. Abdelrazik, "Dielectric properties of snow in the 3 to 37 GHz range," *IEEE Transactions on Antennas and Propagation*, Vol. 34, No. 11, pp. 1329–1340, November 1986.

[25] A. Kovacs, A. J. Gow, and R. M. Morey, "The in-situ dielectric constant of polar firn revisited," *Cold Regions Science and Technology*, Vol. 23, pp. 245–256, 1995.

[26] A. D. Frolov and Y. Y. Macheret, "On dielectric properties of dry and wet snow," *Hydrological Processes*, Vol. 13, pp. 1755–1760, 1999.

[27] C. Matzler, "Microwave permittivity of dry snow," *IEEE Transactions on Geoscience and Remote Sensing*, Vol. 34, No. 2, pp. 573–581, March 1996.

[28] D. M. Pozar, *Microwave Engineering*, 4th Edition, John Wiley & Sons, 2012.

[29] B. A. Atayants, V. M. Davydochkin, V. V. Ezerskiy, V. S. Parshin, and S. M. Smolskiy, *Precision FMCW Short-Range Radar for Industrial Applications*, Artech House, 2014.

[30] M Beniston, "Variations of snow depth and duration in the Swiss Alps over the last 50 years: Links to changes in large-scale climatic forcings," *Climatic Change*, Vol. 36, No. 3-4, pp. 281-300, August 1997.

[31] M. A. Richards, J. A. Scheer, and W. A. Holm, *Principles of Modern Radar – Basic Principles*, SciTech Publishing, 2010.

[32] P. Pouliguen, R. Hemon, C. Bourlier, J. F. Damiens, and J. Saillard, "Analytical formulae for radar cross section of flat plates in near field and normal incidence," *Progress In Electromagnetic Research*, Vol. 9, pp. 263–279, 2008.

[33] P. F. Espin-Lopez and M. Pasian, "Compact 3D-printed variable-infill antenna for snow cover monitoring," *12th European Conference on Antennas and Propagtion*, London, United Kingdom, 9–13 April 2018.

[34] P. F. Espin-Lopez, M. Pasian, M. Barbolini, and F. Dell'Acqua "Optimization of a multi-receiver FMCW radar for snow cover monitoring," *12th European Conference on Antennas and Propagation*, London, United Kingdom, 9–13 April 2018.